Available online at www.sciencedirect.com
ScienceDirect
Trans. Nonferrous Met. Soc. China 34(2024) 2204−2218
Transactions of Nonferrous Metals Society of China
www.tnmsc.cn

Ultra-high strength Inconel 718 alloy produced by a novel heat treatment

Rong RAN, Yang WANG , Fu-qiang REN, Yuan-xiang ZHANG,
Feng FANG, Wei-na ZHANG, Guo YUAN, Guo-dong WANG

State Key Laboratory of Rolling and Automation (RAL), Northeastern University, Shenyang 110819, China

Received 4 January 2023; accepted 13 July 2023

Abstract: In order to ameliorate microstructure and optimize properties of Inconel 718 alloy, a novel heat treatment method combining high-temperature ultra-short annealing at 980 °C for 1 min with subsequent double aging was proposed. The results showed that ultra-short annealing generated partially recrystallized microstructure and recrystallized nuclei were formed even in deformed grains, which was confirmed by KAM maps. Therefore, high-temperature ultra-short annealing overcame recrystallization barrier, and the subsequent recrystallization process could be completed during aging treatment with relatively low temperature, resulting in the uniformly refined microstructure (~3.59 μm). The 980-1min-aged sample exhibited outstanding tensile properties. The room temperature ultimate strength and total elongation were 1600 MPa and 19%, respectively. The corresponding values of high-temperature (650 °C) tensile tests were ~1350 MPa and ~26%. Consequently, ultra-short annealing can be a promising route to enhance the properties of Inconel 718 alloy.

Key words: Inconel 718 alloy; ultra-high strength; δ precipitates; recrystallization behavior; aging treatment

1 Introduction

Inconel 718 alloy, one of the most common nickel-based superalloys, exhibits excellent mechanical properties even up to ~650 °C [1,2]. It has been intensively used in the aerospace, nuclear and petroleum industries due to its excellent properties such as high temperature strength, excellent oxidation resistance and fatigue resistance [3,4].

The mechanical properties are of crucial importance for Inconel 718 alloy because Inconel 718 alloy is a key material in aircraft engines, oil and gas industries, and all of these require excellent combination of strength and elongation. In order to further satisfy the requirements, researchers have put significant efforts into processing parameters design to obtain the best combination of mechanical properties [5,6]. For the Inconel 718 alloy, heat treatment is an essential approach to improve the performance of the final material [7,8]. Although there are many researches on the heat treatment processes of Inconel 718 alloy, most of them are focused on the heat treatment after hot deformation such as forging and hot rolling. And three kinds of heat treatment processes are considered, which are solution heat treatment, standard heat treatment and direct aging treatment. However, there are few studies on the heat treatment process after cold deformation [9]. Heat treatment can greatly influence the grains size distribution of the cold-rolled Inconel 718 alloy, which plays an important role in adjusting the mechanical properties of the material [10]. According to CHEN et al [11], although equiaxed grains can replace deformed grains, it also generates coarse grains during the annealing treatment, which is not

Corresponding author: Yang WANG, Tel: +86-15242086602, E-mail: wangyang@ral.neu.edu.cn;
Guo YUAN, Tel: +86-13609880996, E-mail: yuanguoneu@163.com
DOI: 10.1016/S1003-6326(24)66535-0

conductive to the improvement of mechanical properties. Many researches [12,13] reported that annealing treatment would generate inhomogeneous mixed grains in the sample, causing the deterioration of tensile properties. On the other hand, the previous study shows that appropriate heat treatment can ameliorate the microstructure of the annealed sample after cold rolling, and the uniformly refined grains can be obtained by tailoring the annealing process, which contributed to the enhanced tensile properties [14]. Therefore, it is important to find a proper heat treatment method to uniformly refine the microstructure after cold deformation, which is required for the improvement of mechanical properties [15].

In general, the heat treatment after cold deformation was aimed to eliminate deformed structure generated by previous cold rolling through the occurrence of recrystallization [11]. For Inconel 718 alloy, the recrystallization annealing treatment was often accompanied by the precipitation of δ phase, because the temperature range of the precipitation of δ phase is relatively wide, which is from 750 to 1020 °C [16]. Besides, it should be mentioned that the precipitation of δ particles would compete with recrystallization during annealing, leading to inhomogeneous microstructure and mixed grains. On the other hand, although the recrystallization annealing at higher temperature (>1020 °C) can avoid the precipitation of δ particles, coarser grains are generated due to the increased grain growth rate, which also leads to a degradation in mechanical properties. In contrast, if the growth of recrystallized grains occurred during double aging treatment, the slow growth rate of recrystallized grains would be achieved because of the relatively low aging temperature (i.e. 720 and 620 °C), and as a result, the aged sample could consist of refined recrystallized grains. Furthermore, the ductility of the aged sample still can be maintained when complete recrystallization occurs during the double aging treatment. MAO and ZHAO [17] have reported that annealing at high temperature for short duration can generate recrystallized nuclei even in the deformed grains, which can overcome the recrystallization barrier, and thus promote the recrystallization of the sample subjected to subsequent heat treatment. Therefore, the recrystallization process can be divided into two steps, that is, recrystallized nuclei quickly formed at high temperature and slow grain growth at low temperature. In this way, Inconel 718 alloy may achieve desirable microstructure through the recrystallization process.

In this study, a novel heat treatment process combining high-temperature ultra-short annealing and double aging treatment was proposed to optimize the microstructure of Inconel 718 alloy. The present work aims to explore the processing−structure−property correlations, and to find a suitable processing route for Inconel 718 alloy to achieve excellent tensile properties at both high temperature and room temperature.

2 Experimental

The chemical composition (wt.%) of the present experimental Inconel 718 alloy is: 51.62Ni−19.70Cr−5.42Nb−3.15Mo−0.91Ti−0.685Al−0.013C−(bal.)Fe. The as-received Inconel 718 alloy round bar was forged and hot-rolled into sheets with a thickness of 3 mm. The hot-rolled sheet was firstly solution treated at 1050 °C for 35 min and then air cooled to room temperature. Subsequently, the solution-treated sheet was subjected to cold rolling, and the thickness reduction was 60% (from 3 to 1.2 mm). Then, the cold-rolled sheet was annealed at 980 °C for 1 min and 30 min, respectively. After that, both the cold-rolled and annealed samples underwent double aging treatment, including holding at 720 °C for 8 h, followed by furnace cooling to 620 °C at 50 °C/h and holding at 620 °C for 8 h, and then air quenching to room temperature. Those aged samples were referred as 980-0-aged, 980-1min-aged and 980-30min-aged sample, respectively.

Specimens were observed by OLYMPUS−BX53 M optical microscope (OM), Zeiss GEMINI 300 field emission scanning electron microscope (SEM) equipped with an electron backscattered diffraction (EBSD) system and JXA−8530F electron probe microanalyzer (EPMA). The samples for OM and EPMA analysis were mechanically polished and chemically etched with a solution of H_2O_2 + HCl + C_2H_5OH. The samples analyzed by EBSD were electropolished with an electrolyte composed of perchloric acid and alcohol. The SmartLab9KV X-ray diffractometer (XRD) was used to calculate the fraction of δ phase. The polishing process of the XRD samples is similar to

that of EBSD samples. In order to detect the detailed microstructure features of Inconel 718 alloy, transmission electron microscopy (TEM) analysis was performed. The TEM samples were ground into discs with thickness of 50 μm and diameter of 3 mm, and then double-jet electropolished by 10% perchloric acid and 90% alcohol. The Image-Pro-Plus software was employed for the measurements.

Tensile tests were conducted at both room temperature and high temperature (650 °C). The hot tensile specimens (15 mm (gauge length) × 5 mm (width) × 1.2 mm (thickness)), and the room temperature tensile specimens (10 mm (gauge length) × 5 mm (width) × 1.2 mm (thickness)) were cut from the aged sheets along the rolling direction. Three tensile samples were tested for each condition and the tensile rate was 2 mm/min. Besides, the high temperature tensile samples were heated to 650 °C and held for 5 min in order to eliminate temperature gradient.

3 Results

3.1 Microstructure evolution

The microstructures of the hot-rolled and solution-treated Inconel 718 alloy are shown in Fig. 1. From the OM observation in Fig. 1(a), the grains in hot-rolled sample were slightly elongated along the rolling direction. Since the hot-rolling temperature was higher than the solvus temperature of δ phase, almost no δ particles precipitated in the matrix (Fig. 1(b)). Besides, some carbides dispersed in the matrix (indicated by red arrows), because the solution temperature (1050 °C) was insufficient to dissolve carbide. Inconel 718 alloy has very low total C content and thus the formation of carbide would consume a minimum amount of Nb element. Therefore, the influence of carbides on mechanical properties was not considered in the present work. The solution-treated microstructure is displayed in Fig. 1(c). Equiaxed grains could be seen in the sample, and the average grain size was about 77.3 μm. Besides, some annealing twins could be observed in the sample.

Figure 2 displays the microstructure of cold-rolled sample. It was illustrated that equiaxed grains were replaced by elongated grains after cold rolling. The microstructure was relatively homogeneous except for the carbides. Besides, plenty of shear bands were formed during the cold

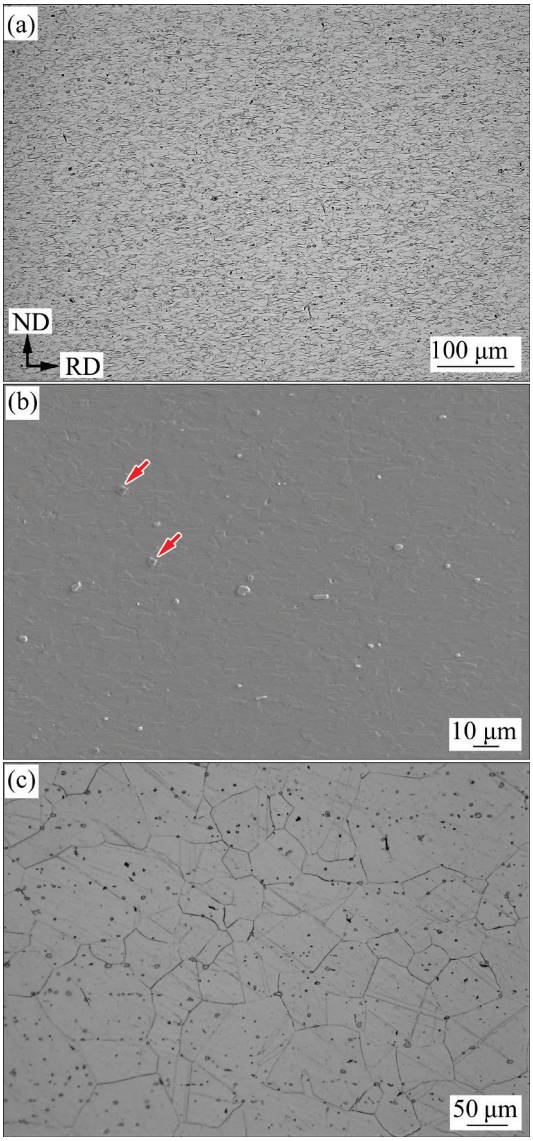

Fig. 1 Microstructures of hot-rolled and solution-treated Inconel 718 alloy: (a, b) OM image and EPMA image of hot-rolled sample; (c) OM image of solution-treated sample (RD is the rolling direction and ND is the normal direction)

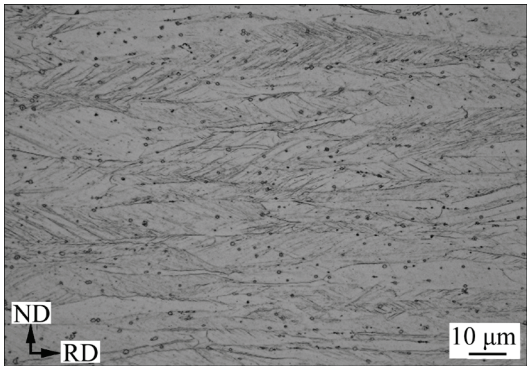

Fig. 2 OM image of cold-rolled Inconel 718 alloy with reduction of 60%

deformation, and the orientation between the rolling direction and the shear bands was about 30°. Additionally, no second-phase particles precipitated during cold rolling, and only grain deformation occurred.

The microstructures of annealed samples are illustrated in Fig. 3. As depicted in Fig. 3(a), the cold-rolled sample after annealing at 980 °C for 1 min comprised both elongated deformed grains and freshly recrystallized grains. In contrast, it can be seen from Fig. 3(b) that when the annealing treatment was performed at 980 °C for 30 min, complete recrystallization occurred and almost no deformed grains remained in the sample. Figures 3(c, d) show magnified images corresponding to Figs. 3(a, b), respectively. Partially recrystallized microstructure could be seen from Fig. 3(c), which was in good agreement with OM microstructure. Besides, it could be observed from Fig. 3(d) that many granular δ particles precipitated in the sample and most of them precipitated along the grain boundaries (indicated by red arrows). In contrast, very few δ phase existed in the sample annealed at 980 °C for 1 min (Figs. 3(a, c)), which could be ascribed to the short duration of the annealing treatment.

The EBSD analysis was performed to further investigate the microstructure evolution. The IPF (inverse pole figure) maps and KAM (kernel average misorientation) maps of cold-rolled sample and annealed samples are shown in Fig. 4. In general, KAM map can be used to embody the local strain distribution of the material according to the change of color in the map [18]. The KAM value is associated with the density of defects such as dislocations or microscopic strain in the sample. The microstructure of cold-rolled sample is displayed in Figs. 4(a, d). The cold-rolled sample was completely composed of deformed structure, and almost no recrystallization occurred (Fig. 4(a)). The highest KAM value and the extensive green regions also confirmed that dislocations were remained in the matrix (Fig. 4(d)). Figures 4(b, e) show the microstructure of the sample annealed at 980 °C for 1 min. It can be seen from Fig. 4(b) that partially recrystallized microstructure existed in the sample, freshly equiaxed grains were formed along previous deformed grain boundaries, and the average size of recrystallized grains was about 1.52 μm. Figure 4(e) exhibits the KAM map of the sample annealed at 980 °C for 1 min. The deformed grain boundaries had high deformation stored energy, which could provide favorable conditions for the nucleation of freshly recrystallized grains. Therefore, recrystallized grains were preferentially formed in those areas, corresponding to blue regions in the center of KAM map. Interestingly, there were also some scattered blue regions in Fig. 4(e) (marked with red circles), which were distinguished from recrystallized regions described

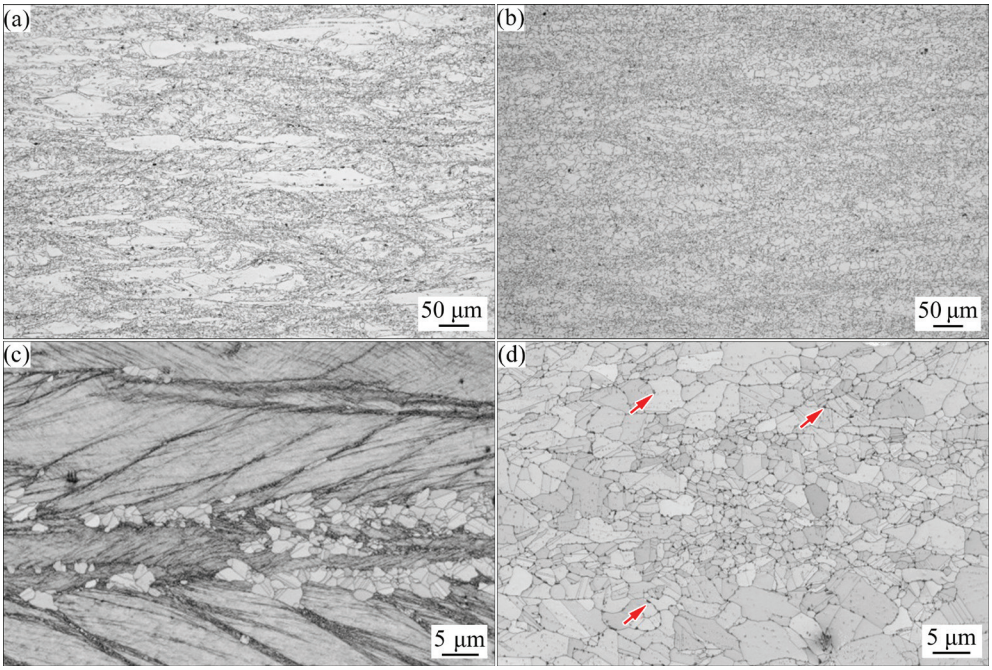

Fig. 3 Microstructures of annealed samples: (a, c) Annealed at 980 °C for 1 min; (b, d) Annealed at 980 °C for 30 min

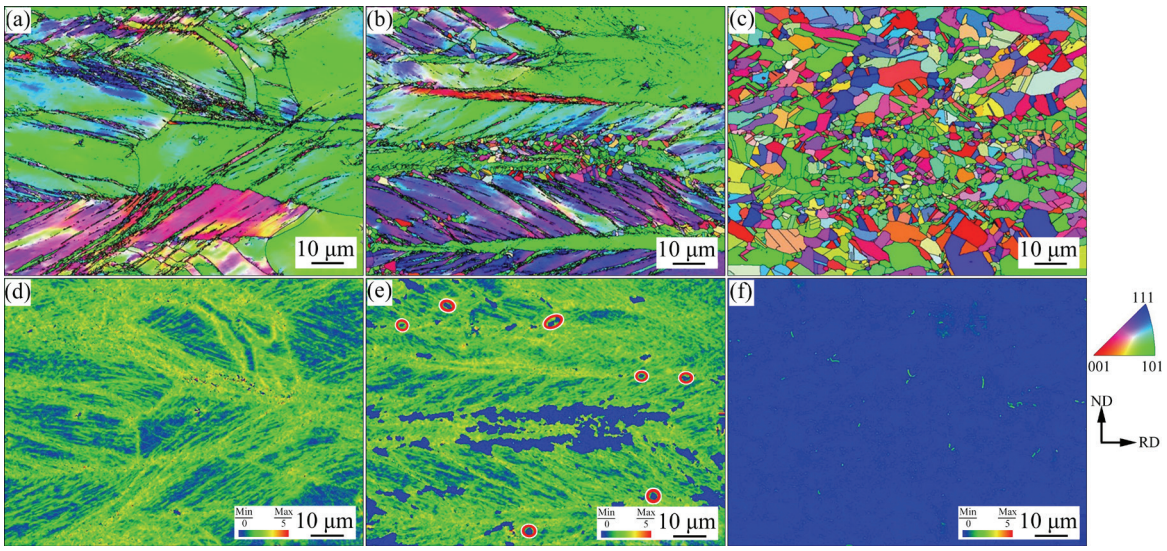

Fig. 4 EBSD analysis results of cold-rolled sample and annealed samples: (a, d) IPF and KAM maps of cold-rolled sample; (b, e) IPF and KAM maps of (980 °C, 1 min) annealed sample; (c, f) IPF and KAM maps of (980°C, 30 min) annealed sample

above. These marked bule regions could be found in deformed grains, which meant that dislocation recovery occurred and recrystallized nuclei were generated in the deformed grains. This phenomenon suggested that annealing at 980 °C for 1 min could overcome the recrystallization barrier to a certain extent. For the sample undergoing annealing treatment at 980 °C for 30 min, as seen in Figs. 4(c, f), complete recrystallization occurred and the corresponding recrystallization fraction was about 93.69%. However, the distribution of grain size was not uniform. According to Fig. 4(c), fine grains were surrounded by large grains and grain size increased from 1.54 to 16.48 μm. The heterogeneous grains would have a negative effect on the mechanical properties of the material. Besides, numerous annealing twins within the austenite matrix were readily observed from Fig. 4(c). The KAM map corresponding to Fig. 4(c) is shown in Fig. 4(f). Less misorientation in Fig. 4(f) confirmed that the dislocations and microscopic strains generated by cold deformation were annihilated during this annealing process.

Then, double aging treatment was carried out on the cold-rolled sample and annealed samples. The microstructures of aged samples are shown in Fig. 5. It is worth noting that the ultra-short annealed sample was almost fully recrystallized after double aging treatment, while the microstructure of cold-rolled sample after the aging treatment remained deformed. It can be seen from Fig. 5(a) that the 980-0-aged sample also consisted of elongated deformed grains and almost no recrystallized grains were found. There was no obvious difference of grain morphology between cold-rolled sample and 980-0-aged sample. Figures 5(b, d, f) exhibit the distributions of various grains of 980-0-aged, 980-1min-aged and 980-30min-aged samples, where recrystallized, substructured and deformed grains were represented by blue, yellow and red regions, respectively. As shown in Fig. 5(b), most of the grains (~96.42%) were deformed grains, indicating the deformed structure retained in the 980-0-aged sample. On the contrary, the 980-1min-aged sample exhibited completely recrystallized microstructure. As estimated from EBSD data in Fig. 5(d), the recrystallization fraction was about 96.84%. Many annealing twins could be observed in the sample (Fig. 5(c)), which also indicated that the sample previously annealed at 980 °C for 1 min underwent static recrystallization during the double aging treatment [19]. Figures 5(e, f) exhibit the microstructure of 980-30min-aged sample. Because recrystallization occurred during previous annealing at 980 °C for 30 min, the 980-30min-aged sample maintained fully recrystallized structure after aging treatment. The fractions of grain types of aged samples are summarized in Fig. 6, indicating that fully recrystallized structure could be obtained in the 980-1min-aged sample. Generally speaking, it is hard for deformed Inconel 718 alloy to recrystallize

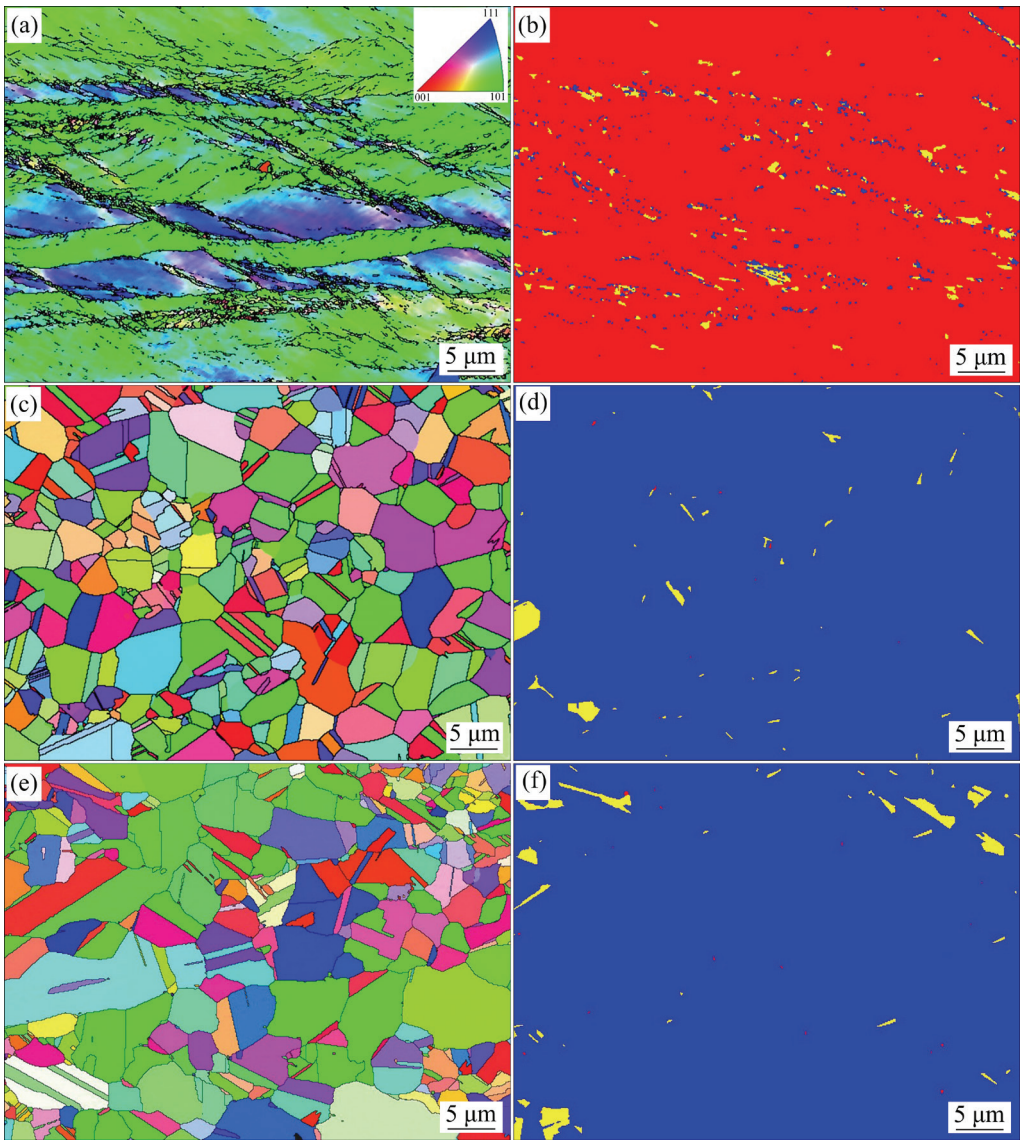

Fig. 5 EBSD analysis results of aged samples: (a, c, e) IPF maps; (b, d, f) Distribution of deformed (red), substructured (yellow) and recrystallized (blue) grains; (a, b) 980-0-aged sample; (c, d) 980-1min-aged sample; (e, f) 980-30min-aged sample

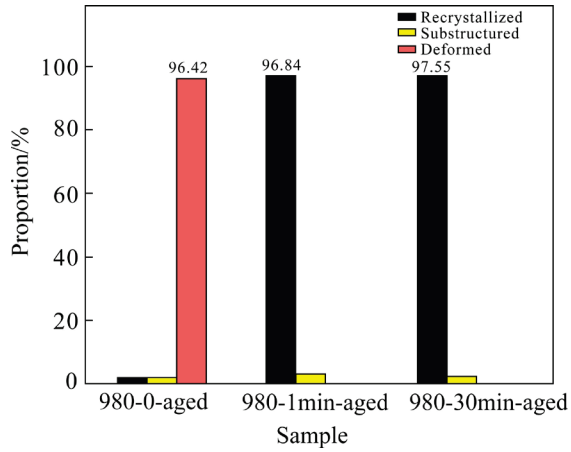

Fig. 6 Relative proportions of different types of grains for aged samples

through the double aging treatment. However, in the present study, annealing at 980 °C for 1 min endowed the sample with partially recrystallized microstructure. More importantly, there were many recrystallized nuclei generated even in the deformed grains of the partially recrystallized sample, which can be confirmed by the KAM map in Fig. 4(d). Therefore, the ultra-short annealing at high temperature could serve to overcome the recrystallization barrier, thus prompting the recrystallization process of the sample subjected to subsequent heat treatment. As a result, for the 980-1min-aged sample, recrystallization could be completed during double aging treatment.

In order to evaluate the grain size uniformity, the corresponding grain diameter distribution histograms are shown in Fig. 7. Obvious difference of the grain size distribution of aged samples could be seen from Fig. 7. The statistical data exhibited that the grain size of 980-30min-aged sample ranged from 1 to 17 μm, and the average grain size was about 7.78 μm. Besides, there was a bimodal distribution of grain size in Fig. 7(b), about 16.1% small grains were 2−3 μm, and there were also some large grains (~17.4%) with size of 11−12 μm. Hence, the grain size of 980-30min-aged sample had a wide distribution rather than a uniform distribution. As for 980-1min-aged sample, it could be observed from Fig. 7(a) that the grain size distribution was relatively concentrated, and most of the grains were between 2 and 3.5 μm. About 46.3% of the grains were close to the average grain size, suggesting that the grain size distribution in this sample was uniform. The average grain size was ~3.59 μm, which was refined in comparison with 980-30min-aged sample. As a result, 980-1min-aged sample has optimized microstructure with uniformly refined grains, which contributed to the excellent tensile properties of the final aged material.

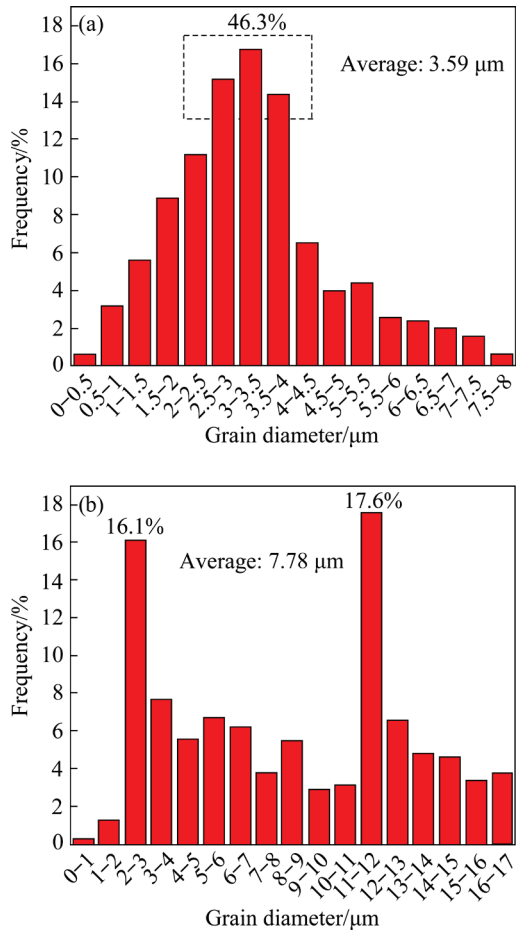

Fig. 7 Grain size distribution of aged samples: (a) 980-1min-aged sample; (b) 980-30min-age sample

The KAM distribution of aged samples is shown in Fig. 8. As mentioned before, KAM is often used to measure the misorientation of local grains in the material and estimate the dislocation density in grains. It is known that the higher the KAM value, the higher the defect density in the matrix. As could be seen in Fig. 8, high KAM value still existed in the microstructure of 980-0-aged sample, which was resulted from the non-recrystallized deformed grains, and the corresponding average KAM value was ~1.69°. In contrast, the KAM values of 980-1min-aged and 980-30min-aged samples were much lower and these two samples showed similar results of the distribution of KAM. According to Fig. 8, the 980-1min-aged sample had a peak value of ~0.25° and the peak of 980-30min-aged sample was located slightly lower around 0.15°. Therefore, it can be concluded that although recrystallization occurred in both annealed samples after double aging treatment, the KAM value of ultra-short annealed sample after aging still higher, causing superior strength in the material. In consequence, the ultra-short annealing together with double aging treatment can be an effective method to refine the grain size and obtain uniform recrystallized microstructure.

3.2 Mechanical properties of Inconel 718 alloy

3.2.1 Hardness

Figure 9 shows the evolution of hardness for cold-rolled, annealed and aged samples. As seen in

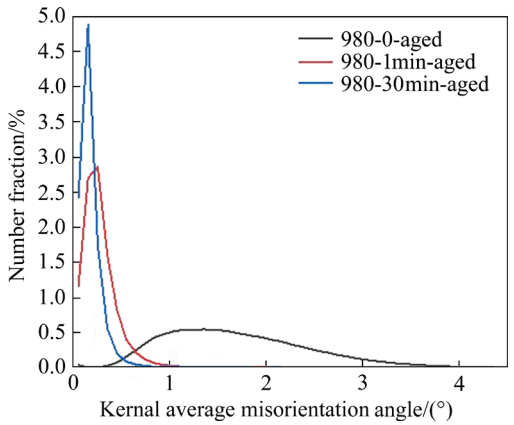

Fig. 8 KAM value vs number fraction curves of different aged samples

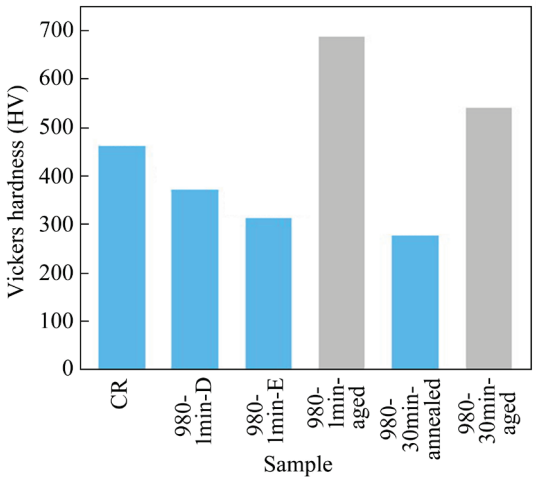

Fig. 9 Vickers hardness change in Inconel 718 alloy samples

Fig. 9, the hardness decreased after annealing treatment, and then increased greatly after double aging. The cold-rolled (CR) sample exhibited the highest hardness of HV 461. After ultra-short annealing at 980 °C for 1 min, the remained deformed grains (referred as 980-1min-D) showed the hardness of HV 371, while the hardness of the equiaxed grains (referred as 980-1min-E) was decreased to HV 312. The sample annealed at 980 °C for 30 min (980-30min-annealed) displayed the lowest hardness of HV 276, which could be ascribed to the fully recrystallized structure with coarse grains. When the annealed samples were subjected to double aging treatment, their hardness was significantly enhanced. It could be seen from Fig. 9 that the 980-1min-aged sample had the highest hardness of HV 687 and the hardness of HV 540 can be observed in the 980-30min-aged sample.

3.2.2 Tensile properties

In order to further illustrate the influence of ultra-short annealing on the mechanical properties of Inconel 718 alloy, the room temperature and high temperature (650 °C) tensile tests were carried out. The obtained tensile curves are shown in Fig. 10. It could be seen from Fig. 10 that the annealing treatment could exert great influence over the tensile properties. When the 980-1min-aged sample was subjected to room temperature deformation, the ultimate strength and total elongation were about 1598.32 MPa and 19.01%, respectively. In comparison with 980-1min-aged sample, the ultimate strength of the 980-30min-aged sample (about 1535.14 MPa) was decreased by 63.18 MPa, while the value of elongation was increased slightly (~20.04%). For the high-temperature tensile properties, the performance of 980-1min-aged sample was still superior to that of 980-30min-aged sample. The values of ultimate strength and total elongation of 980-1min-aged sample were ~1350.25 MPa and ~26.45%, respectively. The corresponding values of 980-30min-aged sample were about 1176.06 MPa and 22.01%. Therefore, high-temperature ultra-short annealing followed by double aging treatment was an effective and economical way to optimize the properties of Inconel 718 alloy.

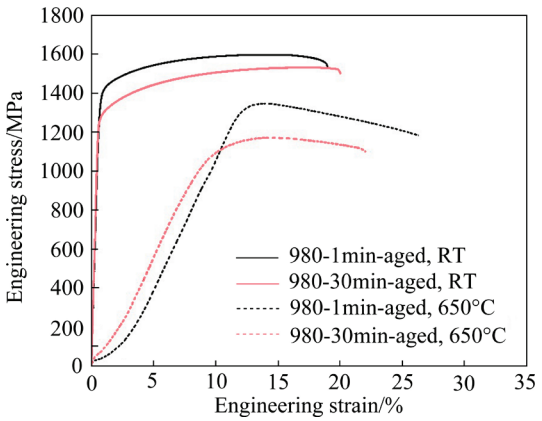

Fig. 10 Engineering stress−strain curves of different samples

3.3 Fracture analysis

The fracture morphology of aged samples is shown in Fig. 11. The fracture surfaces of samples tested at elevated temperature (i.e. 650 °C) were similar to those of samples tested at room temperature. According to Figs. 11(a, b), the fracture surfaces were composed of equiaxed dimples, indicating that ductile characteristic occurred in all conditions, which also corresponded to good elongation in the aged Inconel 718 alloy. On the other hand, Fig. 11(b) showed that many particles distributed in the dimples, as shown by orange arrows. The EPMA analysis indicated that the composition of the particles was 57.25Ni−9.47Fe−12.53Cr−16.59Nb−4.16Mo (at.%), and these particles were rich of Ni and Nb and their atomic ratio was about 3:1, which can be deduced as δ particles. The morphologies near the fracture surface in the longitudinal section of 980-1min-aged and 980-30min-aged samples are displayed in Figs. 11(c, d). The 980-1min-aged sample had

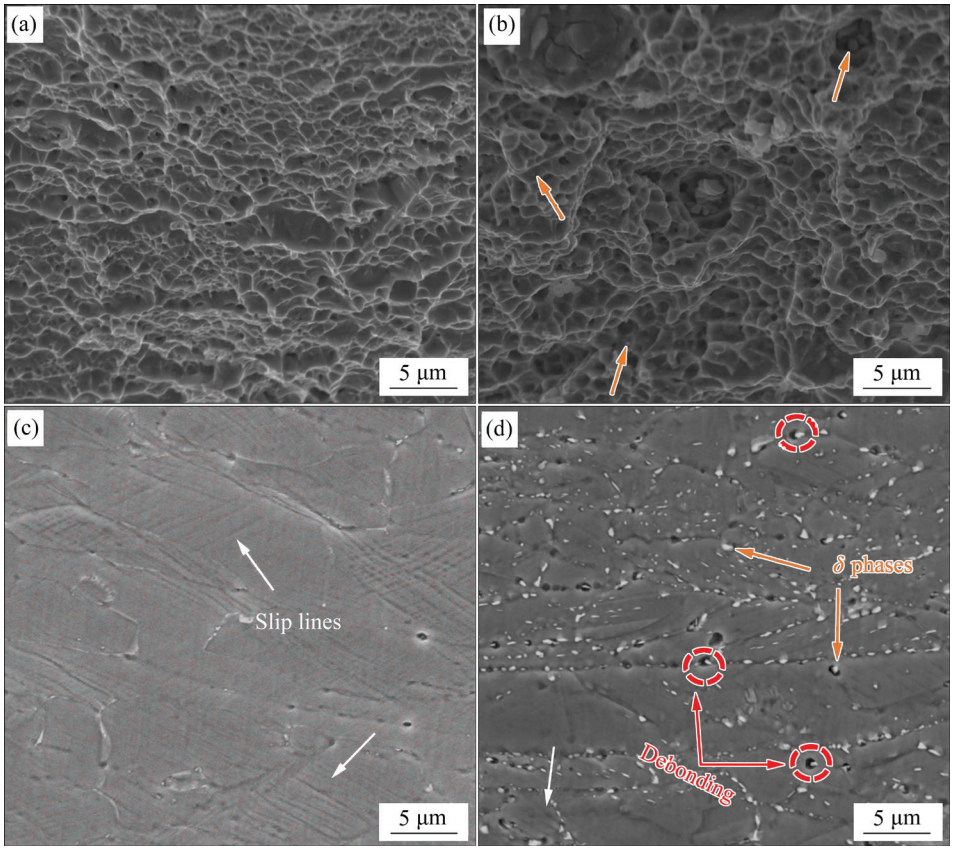

Fig. 11 Room temperature tensile fracture morphology of fracture surface (a, b) and near fracture surface (c, d): (a, c) 980-1min-aged sample; (b, d) 980-30min-aged sample

intensive slip lines which were indicated by white arrows. Although some slip lines could also be observed in the 980-1min-aged sample, marked by white arrow in Fig. 11(d), the number of visible slip lines were less. Besides, it could be seen from Fig. 11(d) that many δ phases at grain boundaries were separated from the matrix. In this case, δ phase at grain boundaries would induce the precipitate debonding from the matrix and promoted the formation of void-formed cracks. Moreover, according to the research [20], the δ phase was brittle and hard; therefore, δ particles might provide favorable condition for the nucleation of micro-void and the propagation of macroscopic cracks, which would adversely affect the elongation.

4 Discussion

4.1 Recrystallization process during primary annealing and double aging

In the present study, the ultra-short annealing at 980 °C for 1 min had significant effects on the microstructure of double-aged Inconel 718 alloy. The uniformly refined microstructure of the final aged sample could be attributed to the high-temperature ultra-short annealing treatment. The microstructure evolution during annealing and double aging treatment is displayed in Fig. 12. As seen from Fig. 12(a), elongated grains and dense dislocations existed in the cold-rolled sample. The grains in solution-treated sample were relatively coarse, and these coarse grains with various orientations would undergo different deformation degrees during cold rolling process. Therefore, the deformation energy storage may vary from grain to grain, leading to different dislocation densities in the grains. Those grains with higher dislocation density were marked by orange dash line in Fig. 12.

During annealing at 980 °C, the nucleation of recrystallized grains was accelerated in the regions with high deformation energy storage, and refined freshly-recrystallized grains preferentially appeared in these regions (Fig. 12(d)). More importantly, many recrystallized nuclei were formed in the original deformed grains during the early stage of

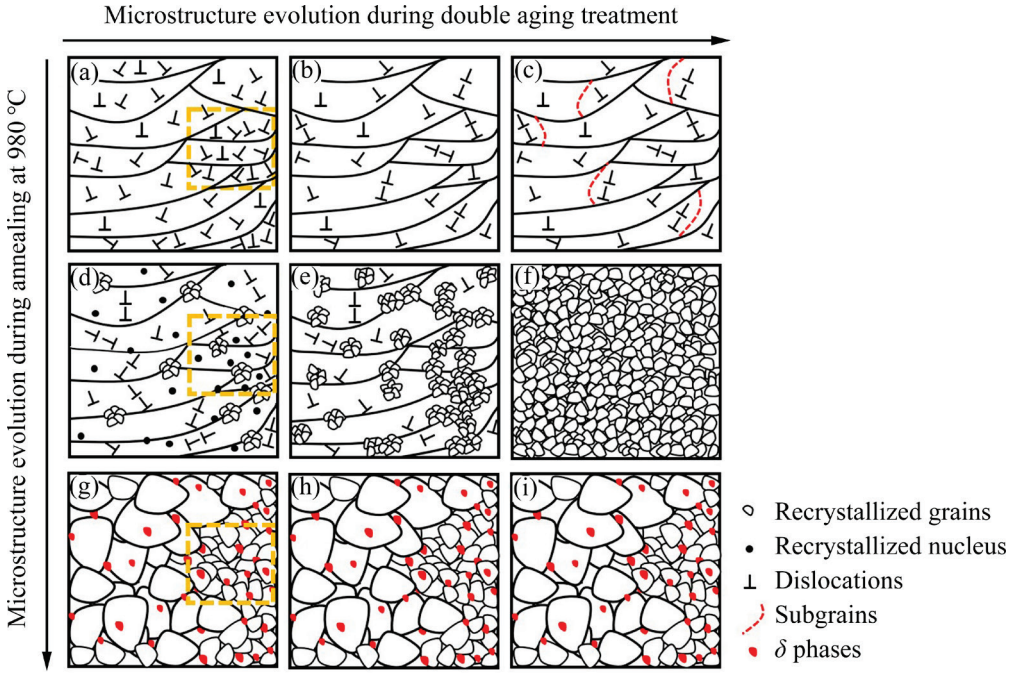

Fig. 12 Schematic illustration of microstructure evolution during annealing and double aging process

annealing at 980 °C, especially in the grains with high deformation energy storage. This phenomenon can be confirmed by the KAM map in Fig. 4(e), where blue regions also appeared in the non-recrystallized grains. Moreover, the evolution of hardness in Fig. 9 further confirmed that dislocation recovery and recrystallized nuclei occurred in the deformed grains during annealing, since the hardness of cold-rolled structure (HV 461) was 24.1% higher than that of the elongated grains in the annealed sample at 980 °C for 1 min (HV 371). In contrast, for the recrystallized refined grains in this annealed sample, the hardness was further decreased to HV 312. Finally, the sample annealed at 980 °C for 1 min consisted of refined equiaxed recrystallized grains and remained deformed grains with many recrystallized nuclei (Fig. 12(d)). With the extension of annealing time, recrystallization gradually occurred in these grains with lower deformation energy. However, due to the low recrystallization nucleation rate, the recrystallized grains became coarse during the high-temperature annealing process. As a result, when annealing at 980 °C for 30 min, although complete recrystallization occurred, the grain size distribution was not uniform (Fig. 12(g)). Besides, when the annealing time was extended to 30 min, there were some granular δ particles precipitated at the grain boundaries, as shown by red particles in Fig. 12(g).

The aged microstructures of the samples subjected to various annealing treatments were totally different. For the cold-rolled sample, since the annealing temperature was much lower than the recrystallization temperature, it was hard for the sample to recrystallize. Therefore, only dislocation recovery could be observed during the whole aging process. It can be seen from Fig. 12(b) that the dislocation came over the pinning effect of the deformed structure and dislocation rearrangement happened. Also, the dislocation density was decreased due to dislocation annihilation. With the extension of the aging process, some sub-grain boundaries would appear, as seen from Fig. 12(c). As a result, the cold-rolled sample after aging treatment remained deformed structure. In contrast, the microstructure of 980-1min-aged sample was composed of equiaxed recrystallized grains, which could be attributed to the ultra-short annealing at 980 °C for 1 min. As mentioned before, the annealing with high temperature and short duration could generate recrystallized nuclei even in the deformed grains. Then, these newly formed recrystallized nuclei could evolve into freshly recrystallized grains even at aging temperature (Fig. 12(e)). After that, these freshly-refined grains experienced slow grain growth during double aging

process. Finally, 980-1min-aged sample consisted of homogenous refined grains (Fig. 12(f)). As for the sample previously annealed at 980 °C for 30 min, full recrystallization occurred during the annealing, and the aged sample inherited the heterogeneous recrystallized grains (Fig. 12(i)).

4.2 Influence of primary ultra-short annealing on tensile properties

The present results confirmed that ultra-short annealing coupled with double aging treatment can increase the strength of Inconel 718 alloy. The excellent tensile properties of 980-1min-aged sample can be attributed to several reasons.

In Inconel 718 alloy, the δ phase is an important precipitated phase, which can affect the mechanical properties significantly. The influence of δ phase on mechanical properties is complex. On the one hand, the appropriate amount of granular δ phases at grain boundary can be conductive to the improvement of creep resistance and creep ductility [21]. On the other hand, the stress concentration at grain boundaries caused by the pinning effect of δ precipitates can induce the precipitate debonding from the matrix and promote the formation of void-formed cracks, which is disadvantageous to the properties [22]. During annealing at 980 °C, δ phase can precipitate directly from the matrix. The XRD patterns of 980-1min-aged and 980-30min-aged sample are shown in Fig. 13. Three main peaks (i.e. FCC-γ matrix and γ' and γ'' strengthening phases) could be detected in both aged sample. However, because of the high similarity of lattice parameters of the γ', γ'' and γ phases and the overlapping peaks of those phases, it is difficult to distinguish γ' and γ'' phases from FCC-γ matrix. Besides, it was hard to detect the corresponding peaks of carbides due to its low content. It could be seen from Fig. 13 that there was no precipitation peak of phase in the 980-1min-aged sample, which indicated that very few δ particles existed in the sample. It is reasonable that the incubation period of the precipitation of δ phase at 980 °C may be much longer than the holding time in this work (1 min). On the contrary, the XRD pattern of 980-30min-aged sample confirmed that some δ phase particles were precipitated in the sample. According to calculation [23], the fraction of δ phase in the 980-30min-aged sample was about 1.62%.

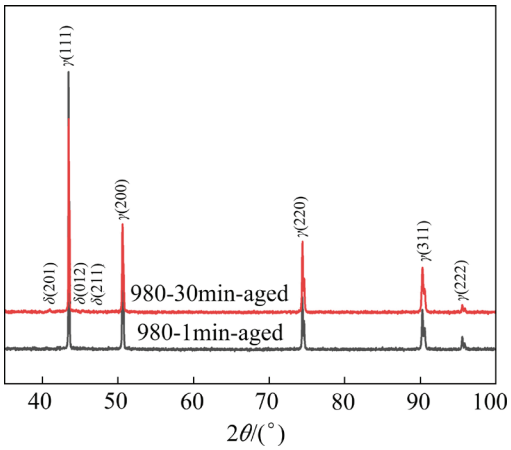

Fig. 13 XRD patterns of different samples

Although the precipitation of δ phases at grain boundary can enhance creep properties, the presence of δ particles does not obviously improve the tensile strength of Inconel 718 alloy [24]. The high strength of Inconel 718 alloy was mainly attributed to the precipitation of γ'' particles. The TEM analysis was performed to further detect the characteristics of precipitates in the aged samples. It could be seen from Fig. 14(a) that numerous nano-sized particles uniformly distributed in the 980-1min-aged sample. The disc-like γ'' phase and spherical-like γ' phase were indicated by red and yellow arrow, respectively. The selected area electron diffraction (SAED) pattern inserted in Fig. 14(a) further confirmed that those precipitates were γ'' and γ'. Besides, the fractions of γ'' and γ' phases in Fig. 14(a) were about 12.53% and 4.38%, respectively. The distribution of the strengthening phases in 980-30min-aged sample could be seen in Fig. 14(b). For the 980-30min-aged sample, the fraction of γ'' phase was ~10.46%, and that of γ' phase was ~4.42%. Figure 14(c) showed that some granular particles precipitated in the 980-30min-aged sample, and the SAED pattern confirmed that these particles were δ phases. The composition of the γ''-Ni_3Nb strengthening phase is the same as that of the δ-Ni_3Nb phase, so the presence of more δ particles in the matrix meant that less γ'' phase could precipitate during aging treatment, which could explain lower fraction of γ'' phase in the 980-30min-aged sample. The γ'' strengthening phase is the major contributor to the strength of Inconel 718 alloy, which can be ascribed to the partial coherency arising from large lattice misfit between γ'' precipitates and matrix. Consequently,

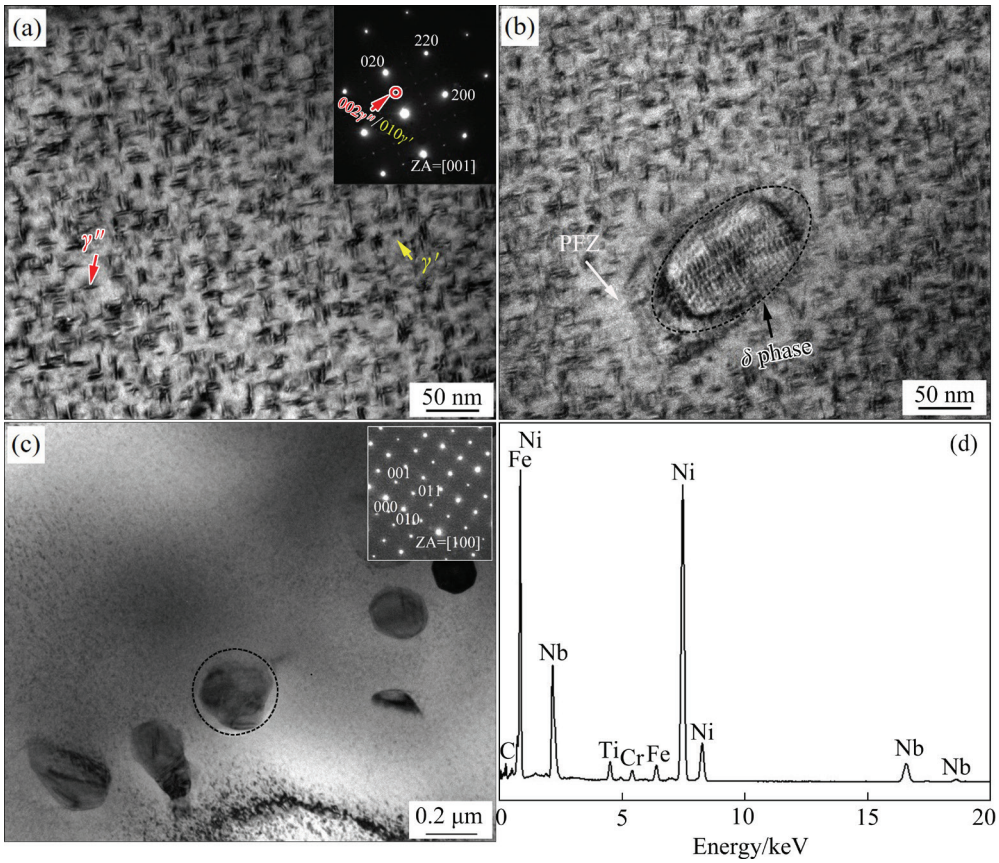

Fig. 14 TEM analysis results of 980-1min-aged sample (a) and 980-30min-aged sample (b, c, d): (a, b) $\gamma''+\gamma'$ phase and SAED pattern taken in [001] zone axis direction; (c) δ phase and SAED pattern taken in [100] zone axis direction; (d) EDS result of δ precipitate in (b)

more γ'' phases precipitated in 980-1min-aged sample were conductive to the improvement of strength.

Besides, the EDS analysis of the precipitate circled by black ellipse in Fig. 14(b) indicated that the chemical composition of the precipitate was 58.47Ni−13.24Fe−9.36Cr−18.02Nb−0.91C (at.%) (Fig. 14(d)). The particle was mainly composed of Ni and Nb elements and the atomic ratio was about 3:1; therefore, it can be deduced that the precipitate was δ phase. The precipitate free zone (PFZ) existed in the vicinity of δ phase, as pointed by white arrow in Fig. 14(b), indicating that the nucleation and growth of γ'' phase were inhibited due to the depleted Nb atoms near the δ phase. It was reported that the formation of PFZ can negatively influence the mechanical properties of Inconel 718 alloy [25]. Therefore, numerous uniformly-distributed γ'' phase in the 980-1min-aged sample was a contributor to the ultra-high strength of Inconel 718 alloy.

Moreover, as the grain size of 980-1min-aged sample (~3.59 μm) was finer than that of the 980-30min-aged sample (~7.78 μm), the grain boundary strengthening in the 980-1min-aged sample was more obvious. Fine-grain structure can impede the movement of dislocations, which is beneficial to the enhancement of strength. To further study the grain structure on deformation behavior of Inconel 718 during tensile test, the EBSD and SEM analyses were performed. The IPF and KAM maps of the longitudinal section near the fracture surface in the 980-1min-aged and 980-30min-aged samples after room temperature tensile test are presented in Fig. 15. Average KAM values of 980-1min-aged and 980-30min-aged sample were about 1.27 and 0.83, respectively. It is reported that the GND (geometrically necessary dislocation) density can be calculated by the KAM value: $\rho=2\theta/(\mu b)$, where θ is the misorientation angle, μ is the step size of EBSD analysis and b is the magnitude of Burgers vector [26]. Therefore, the GND density of 980-1min-aged was higher than that of 980-30min-aged sample. Some grains had

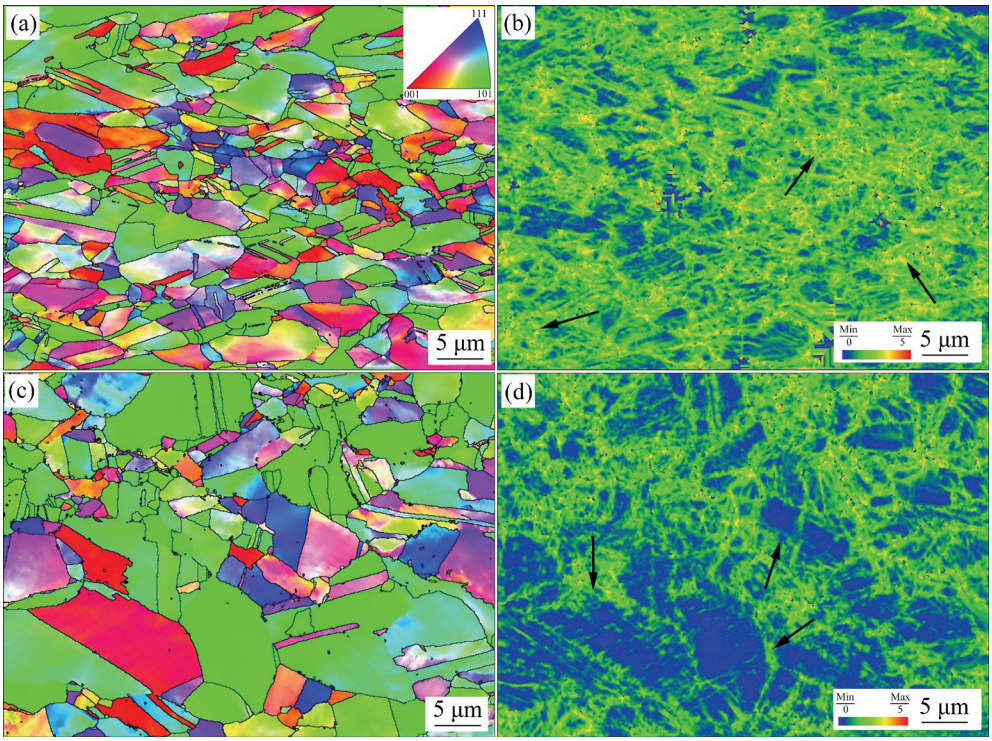

Fig. 15 EBSD IPF and KAM maps (a, c) and SEM images (b, d) of fractures in longitudinal sections of 980-1min-aged sample (a, b) and 980-30min-aged sample (c, d)

high GND densities in the entire grain (marked by arrows in Fig. 15(b)) in the 980-1min-aged sample. In contrast, grains with lower GND density in the interior were dominant in the 980-30min-aged sample, which could be seen from arrows in Fig. 15(d). In this case, more dislocation pile-up occurred in the 980-1min-aged sample during deformation, which also confirmed that the 980-1min-aged sample underwent much more serious plastic deformation during tensile test. As a result, the strength of 980-1min-aged sample was improved.

Additionally, it can be seen from the IPF maps in Figs. 5 and 15 that the grain size distribution of 980-1min-aged sample before and after the deformation was more homogenous. Therefore, the 980-1min-aged sample had better capacity of coordinated deformation and the plastic deformation was more uniform in the sample. According to ZHANG et al [27], inhomogeneous grain size can promote uncoordinated strain and stress concentration, which would cause the crack initiation and propagation. By comparison, more uniform grain structure allowed the grain boundaries and dislocations to slide easily and distribute uniformly. In this case, 980-1min-aged sample could withstand more deformation before the fracture occurred, resulting in a higher elongation [28]. Besides, nearly completely-recrystallized structure was obtained in the 980-1min-aged sample and numerous HAGBs existed in the sample. These HAGBs can impede and block the dislocation, which led to enhanced strain-hardening capacity and improved ductility of the material. Finally, the 980-1min-aged sample exhibited excellent combination of strength and elongation due to the optimized microstructure obtained from the novel heat treatment process.

5 Conclusions

(1) The ultra-short annealing treatment at 980 °C for 1 min could overcome recrystallization barrier, and many recrystallized nuclei were formed even in the deformed grains in this partially recrystallized sample. Therefore, the sample was more likely to recrystallize when subjected to subsequent heat treatment. As a result, fully recrystallized microstructure with uniformly refined grains was obtained after double aging treatment, which was conductive to the optimization of mechanical properties of Inconel 718 alloy.

(2) The proposed novel heat treatment process containing high-temperature ultra-short annealing and double aging treatment could effectively improve the mechanical properties of Inconel 718 alloy. When the tensile test was performed at room temperature, the values of ultimate strength and total elongation were about 1600 MPa and 20%. For the high-temperature tensile properties, the ultimate strength was ~1350 MPa, and the elongation was ~26%.

CRediT authorship contribution statement

Rong RAN: Conceptualization, Formal analysis, Investigation, Writing − Original draft; **Yang WANG:** Conceptualization, Funding acquisition, Resources, Writing − Original draft; **Fu-qiang REN:** Funding acquisition, Methodology; **Yuan-xiang ZHANG:** Investigation, Visualization, Writing − Review & editing; **Feng FANG:** Formal analysis, Methodology, Writing − Review & editing; **Wei-na ZHANG:** Conceptualization, Supervision; **Guo YUAN:** Conceptualization, Project administration, Supervision; **Guo-dong WANG:** Project administration, Supervision, Writing − Review & editing.

Declaration of competing interest

The authors declare that they have no known competing financial interests or personal relationships that could have appeared to influence the work reported in this paper.

Data availability

The raw/processed data required to reproduce these findings cannot be shared at this time as the data also forms part of an ongoing study.

Acknowledgments

This work was financially supported by the National Natural Science Foundation of China (No. 52104372), the Fundamental Research Funds for the Central Universities, China (No. N2107001) and the Postdoctoral Research Foundation of China (Nos. 2019M651129, 2019TQ0053).

References

[1] LIU Bo, DING Yu-tian, XU Jia-yu, CAO Yu-bi, WANG Xing-mao, ZHANG Hong-fei, HU Yong, SUN Fu-hao, Qian-chun. Outstanding strength−ductility synergy in Inconel 718 superalloy via laser powder bed fusion and thermo-mechanical treatment [J]. Additive Manufacturing, 2023, 67: 103491.

[2] SMITH T M, BONACUSE P, SOSA J, KULIS M, EVANS L. A quantifiable and automated volume fraction characterization technique for secondary and tertiary γ' precipitates in Ni-based superalloys [J]. Materials Characterization, 2018, 140: 86−94.

[3] ALMARAZ G M D, TAPIA M G, TELLO I F Z. Ultrasonic fatigue endurance of Inconel 718 after the heat treatments: solution annealing and double aging [J]. Procedia Structural Integrity, 2022, 39: 281−289.

[4] NIYAS S, JAPPES J T, ADAMKHAN M, BRINTHA N C. An effective approach to predict the minimum tool wear of machining process of Inconel 718 [J]. Materials Today: Proceedings, 2022, 60: 1819−1834.

[5] DENG De-wei, WANG Chun-guang, LIU Qian-qian, NIU Ting-ting. Effect of standard heat treatment on microstructure and properties of borided Inconel 718 [J]. Transactions of Nonferrous Metals Society of China, 2015, 25: 437−443.

[6] LI Chen, HODGSON P, PREUSS M, CHEN Yu, WU Xin-hua, ZHU Yu-man, TIAN Yang, HUANG Ai-jun. Rolling-assisted direct energy deposited Inconel 718: Microstructural evolution and mechanical properties after optimized heat treatment [J]. Journal of Materials Science & Technology, 2023, 144: 118−127.

[7] XUE Hao, ZHAO Jing-qi, LIU Yong-kang, ZHANG Chun-xiang, LUO Jun-ting. δ-phase precipitation regularity of cold-rolled fine-grained GH4169 alloy plate and its effect on mechanical properties [J]. Transactions of Nonferrous Metals Society of China, 2020, 30: 3287−3295.

[8] ZHANG Yao-cheng, YANG Li, CHEN Ting-yi, ZHANG Wei-hui, HUANG Xi-wang, DAI Jun. Investigation on the optimized heat treatment procedure for laser fabricated IN718 alloy [J]. Optics & Laser Technology, 2017, 97: 172−179.

[9] LOW Z K, CHAISE T, BARDEL D, CAZOTTES S, CHAUDET P, PEREZ M, NELIAS D. A novel approach to investigate delta phase precipitation in cold-rolled 718 alloys [J]. Acta Materialia, 2018, 156: 31−42.

[10] MEI Yun-peng, LIU Yong-chang, LIU Chen-xi, LI Chong, YU Li-ming, Guo Qian-ying, LI Hui-jun. Effects of cold rolling on the precipitation kinetics and the morphology evolution of intermediate phases in Inconel 718 alloy [J]. Journal of Alloys and Compounds, 2015, 649: 949−960.

[11] CHEN Ming-song, ZOU Zong-huai, LIN Yong-chen, LI Hong-bin, YUAN Wu-quan. Effects of annealing parameters on microstructural evolution of a typical nickel-based superalloy during annealing treatment [J]. Materials Characterization, 2018, 141: 212−222.

[12] GRIBBIN S, GHORBANPOUR S, FERRERI N C, BICKNELL J, TSUKROV I, KNEZEVIC M. Role of grain structure, grain boundaries, crystallographic texture, precipitates, and porosity on fatigue behavior of Inconel 718 at room and elevated temperatures [J]. Materials Characterization, 2019, 149: 184−197.

[13] WANG Guan-qiang, CHEN Ming-song, LIN Yong-chen, LOU Yu-min, LI Hong-bin, MA Yan-yong, ZOU Zong-huai, CHEN Quan, XIA Yu-chi. Effects of double-stage annealing parameters on tensile mechanical properties of initial aging

deformed GH4169 superalloy [J]. Materials, 2021, 14: 4339.
[14] RAN Rong, WANG Yang, ZHANG Yuan-xiang, FANG Feng, XIA Yu-kun, ZHANG Wei-na, YUAN Guo, WANG Guo-dong. Two-stage annealing treatment to uniformly refine the microstructure, tailor δ precipitates and improve tensile properties of Inconel 718 alloy [J]. Journal of Alloys and Compounds, 2022, 927: 166820.
[15] VIKRAM R J, SINGH A, SUWAS S. Effect of heat treatment on the modification of microstructure of selective laser melted (SLM) IN718 and its consequences on mechanical behavior [J]. Journal of Materials Research, 2020, 35: 1949−1962.
[16] TOMAS A, EIWAHABI M, CABRERA J M, PRADO J M. High temperature deformation of Inconel 718 [J]. Journal of Materials Processing Technology, 2006, 177: 469−472.
[17] MAO Wei-min, ZHAO Xin-bing. Recrystallization and grain growth of metals [M]. Beijing: Metallurgical Industry Press, 1994. (in Chinese)
[18] CAO Ming, ZHANG Dong-yun, CAO Yang, CHEN Run-ping, HUANG Guo-liang, FENG Zhe, POPRAWE R, SCHLEIFENBAUM J H, ZIEGLER S. The effect of homogenization temperature on the microstructure and high temperature mechanical performance of SLM-fabricated IN718 alloy [J]. Materials Science and Engineering A, 2021, 801: 140427.
[19] CAO Yu, BAI Pu-cun, LIU Fei, HOU Xiao-hu, GUO Yu-hao. Effect of the solution temperature on the precipitates and grain evolution of IN718 fabricated by laser additive manufacturing [J]. Materials, 2020, 13: 340.
[20] XIAO Hui, XIE Pan, CHEN Man-ping, SONG Li-jun. Enhancing mechanical properties of quasi-continuous-wave laser additive manufactured Inconel 718 through controlling the niobium-rich precipitates [J]. Additive Manufacturing, 2020, 34: 101278.
[21] ZHANG Hong-jun, LI Chong, GUO Qian-ying, MA Zong-qing, HUANG Yuan, LI Hui-jun, LIU Yong-chang. Hot tensile behavior of cold-rolled Inconel 718 alloy at 650 °C: The role of δ phase [J]. Materials Science and Engineering A, 2018, 722: 136−146.
[22] ZHANG Shu-ya, WANG Li-lin, LIN Xin, YANG Hai-ou, LI Ming-hong, LEI Li-ming, HUANG Wei-dong. Precipitation behavior of δ phase and its effect on stress rupture properties of selective laser-melted Inconel 718 superalloy [J]. Composites Part B: Engineering, 2021, 224: 109202.
[23] LIU Wen-chang, XIAO Fu-ren, YAO Mei, CHEN Zong-lin, WANG Shao-gang, LI Wei-hong. Quantitative phase analysis of Inconel 718 by X-ray diffraction [J]. Journal of Materials Science Letters, 1997, 16: 769−771.
[24] AZADIAN S, WEI Liu-ying, WARREN R. Delta phase precipitation in Inconel 718 [J]. Materials Characterization, 2004, 53: 7−16.
[25] XU Jing-hao, MA Tao-ran, PENG Ru-lin, HOSSEINI S. Effect of post-processes on the microstructure and mechanical properties of laser powder bed fused IN718 superalloy [J]. Additive Manufacturing, 2021, 48: 102416.
[26] THESKA F, STANOJEVIC A, OBERWINKLER B, RINGER S P, PRIMIG S. On conventional versus direct ageing of Alloy 718 [J]. Acta Materialia, 2018, 156: 116−124.
[27] ZHANG Shu-ya, LIN Xin, WANG Li-lin, YU Xiao-bin, YANG Hai-ou, LEI Li-ming, HUANG Wei-dong. Influence of grain inhomogeneity and precipitates on the stress rupture properties of Inconel 718 superalloy fabricated by selective laser melting [J]. Materials Science and Engineering A, 2021, 803: 140702.
[28] ZHANG Dong-yun, NIU Wen, CAO Xuan-yang, LIU Zhen. Effect of standard heat treatment on the microstructure and mechanical properties of selective laser melting manufactured Inconel 718 superalloy [J]. Materials Science and Engineering A, 2015, 644: 32−40.

新型热处理方法制备超高强度 Inconel 718 合金

冉 蓉，王 洋，任富强，张元祥，方 烽，张维娜，袁 国，王国栋

东北大学 轧制技术及连轧自动化国家重点实验室，沈阳 110819

摘　要：为改善 Inconel718 合金的组织并优化性能，提出一种 980 ℃，1 min 高温超短退火和随后的双时效相结合的新型热处理方法。结果表明，超短退火处理产生了部分再结晶组织，KAM 图表明即使在变形晶粒中也形成了再结晶晶核。因此，高温超短退火克服了再结晶势垒，使得后续的再结晶过程可以在较低温度的时效处理过程中完成，从而获得了均匀细化的组织(~3.59 μm)。980-1min-aged 样品具有优异的拉伸性能，室温极限强度和总伸长率分别为 1600 MPa 和 19%。650 °C 热拉伸条件下的极限强度和伸长率分别约为 1350 MPa 和 26%。因此，高温超短退火能有效提高 Inconel718 合金的性能。

关键词：Inconel 718 合金；超高强度；δ 相析出相；再结晶行为；时效处理

(Edited by Bing YANG)